A Case Study of Pole-Phase Changing Induction Machine Performance

Konstantina Bitsi[1], and Sjoerd G. Bosga[1,2]
[1]KTH Royal Institute of Technology, Division of Electric Power and Energy Systems, Stockholm, Sweden
[2]ABB Corporate Research, Västerås, Sweden
E-mails: bitsi@kth.se, sjoerd.bosga@se.abb.com

Acknowledgments

This research project is supported in part by the Swedish Energy Agency (Energimyndigheten).

Keywords

≪FEM modeling≫, ≪independently-controlled stator coils≫, ≪induction machine≫, ≪maximum efficiency operation≫, ≪maximum torque per ampere operation≫, ≪phase-changing≫, ≪pole-changing≫.

Abstract

Pole-phase changing (PPC) induction machines (IMs) can achieve improved efficiency as well as wider torque-speed range compared to their fixed pole-phase counterparts. In this paper, a 4-pole IM is designed and evaluated in terms of its pole-phase changing performance.

Introduction

The exponential growth of the global electric vehicle market in recent years represents a significant ongoing environmental sustainable development. In order to provide viable solutions in the competitive automotive industry, the produced electric motors and drivetrain designs need to meet demanding requirements, including high efficiency, increased torque and power density capabilities and a wide high-speed range. Induction machines (IMs) constitute a robust, reliable and rare-earth-free alternative to widely adopted interior permanent magnet synchronous machines [1–3]. However, due to their high values of leakage inductance, they inherently showcase poor flux weakening capability.

To improve the high-speed torque and power output of IMs, leakage-minimization strategies [4, 5], dual drive topologies [6, 7] as well as torque-speed range manipulation methods have been proposed. The latter include also the electronic pole-changing, which involves the utilization of the converter in order to dynamically change the pole number of the machine [8–11]. In accordance with this technique, the wound independently-controlled stator coils (WICSC) machine is introduced in [12]. This topology comprises an asynchronous rotor and individually excited toroidal coils in each stator slot. The adopted stator-winding configuration allows the independent current control of each stator-slot coil and, thus, WICSC topologies exhibit the ability of real-time pole-phase changing (PPC) during operation [13]. To independently control each stator toroidal coil, it should be connected to an individual converter leg, as shown in Fig. 1.

A widely selected pole number for machines used in automotive applications is four, as 4-pole designs offer a good compromise between speed range and torque capability. Therefore, the goal of this paper is to demonstrate the benefits that PPC can offer to the performance of a 4-pole IM, originally intended for fixed pole-phase operation. Specifically, the study will compare the produced torque capability, efficiency and flux-weakening range while operating with a PPC strategy versus typical fixed pole-phase operation.

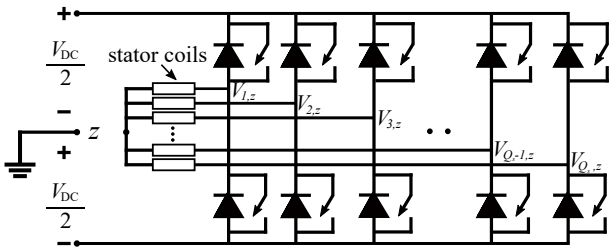

Fig. 1: Schematic of an m-phase bridge-type voltage source inverter.

This paper is organized as follows: in Section II, the design and the electromagnetic model of the examined 4-pole IM are discussed. Section III presents the identification processes of the optimal pole-phase modes based on the selected criteria. In Section IV, the performance of the studied topology as a PPCIM is evaluated in terms of torque-speed capability and efficiency using different operating strategies. The main conclusions are summarized in the final section.

WICSC Electromagnetic Model

The geometry of the investigated WICSC IM is shown in Fig. 2. This geometry is designed within the scope of this analysis for fixed 4-pole operation, following the design algorithm described in [14], with the specifications of Table I as input parameters.

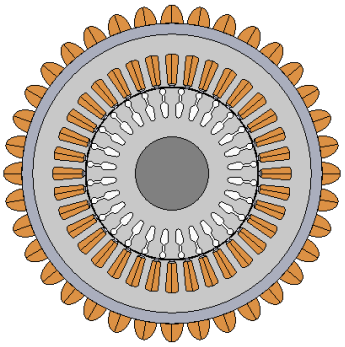

Fig. 2: Geometry of the investigated WICSC IM, originally designed for 4-pole fixed pole-phase operation.

Table I: Geometrical and nominal operating parameters of the original 4-pole IM

Stator outer diameter (mm)	256
Axial length (mm)	200
Torque (Nm)	64
Speed (rpm)	3000
Mechanical power (kW)	20
Number of poles	4

The PPC analysis is performed numerically using 2D FEM models, with sinusoidal stator current supply in each independent coil. The current in each phase n can be defined as [12]

$$i_{s,n} = \hat{\imath}_s \cos\left(\frac{p}{2}\omega_s t - (n-1)\frac{\pi}{m}\right) \tag{1}$$

where $\hat{\imath}_s$ is the stator current amplitude, ω_s the angular electrical frequency, m the number of phases and p the number of poles. The number of stator slots per pole per phase is expressed as

$$q_s = \frac{Q_s}{mp} \tag{2}$$

where Q_s is the number of stator slots. In this study,the parameter q_s is set to unity, to maximize the winding factor and minimize the harmonic content. Therefore, during pole-phase modulation, the highest permissible phase number is selected for a given pole number of the stator current excitation according to (2). It should be noted that with the term ”phase”, we do not mean coils that are connected physically between them, but rather share the current excitation pattern of a typical ”phase” in a conventional IM.

In the FEM implementation, the stator-coil end-winding resistance and inductance are present in the 2D

FEM model, using external electric circuits for all stator toroidal coils. The end-winding inductances are approximated by manipulating the expression for an air-cored solenoid inductance to take into account the presence of iron parts in the vicinity [15]. On the rotor side, the resistances and the inductances of the short-circuit ring elements are included in the FEM model, by implementing an external electric circuit to connect the rotor bars. The end-winding squirrel-cage inductance is estimated based on the method of calculating the self-inductance of an identical circular ring, as in [16].

Optimal Pole-Phase Selection Methods

The first step towards determining the optimal pole-phase selection of a PPC machine at each operating point is to establish the goal of the operating strategy. In this paper, two strategies will be investigated: (a) the maximization of the torque per ampere capability, i.e. maximum extension of the torque-speed envelope, as well as (b) the maximization of the machine efficiency. For these strategies, the appropriate current-contol schemes need to be determined.

Maximum Torque Per Ampere Operation

To accurately specify the pole-phase selection that outputs the highest torque per ampere at each specific operating point, all maximum torque capabilities of the possible pole-phase selections should be determined. For this purpose, the operation of each of these selections should be controlled based on the following schemes:

1. Maximum torque per ampere (MTPA) control: At low speeds, below the maximum voltage imposed by the DC bus voltage limit, the maximum permissible produced torque is only dependent on the current excitation. When i_s is low and the behavior of the iron is linear, the angular slip frequency ω_{slip} in the rotor-flux reference frame can be analytically estimated using the following expression

$$\omega_{\text{slip}} = s\omega_s = \frac{R'_r}{L_m}\frac{i_{sq}}{i_{sd}} \tag{3}$$

   where R'_r is the rotor resistance referred to the stator side in the steady-state equivalent circuit of the IM model [17]. As the current level is increased, saturation becomes more prominent and the machine parameters R'_r and L_m are no more constant [18]. The maximum current limit is imposed by the converter current rating.

2. Flux weakening (FW) control: When the DC bus voltage limit is reached at nominal speed, the voltage of the machine cannot be further increased. Therefore, the stator flux λ_{sd} should be decreased in order for the machine to reach higher speeds, resulting inevitably in a lower maximum torque capability.

3. Maximum Torque Per Volt (MTPV) Control: In the case that both the current and voltage limits must be violated to reach a higher-speed region, λ_{sd} should be further reduced. To achieve this, the operating current level of the machine should be decreased, while remaining at the maximum voltage, and the slip frequency should be reduced accordingly to output the maximum permissible torque.

Maximum Efficiency Operation

Based on the strategy of the the previous section, the most extended torque-speed envelope of the machine can be obtained. Within that envelope, the optimal efficiency map can be determined, by estimating and comparing the total losses of all possible pole-phase selections. For this purpose, the following loss components are considered:

1. Resistive losses: The stator copper losses $P_{\text{Cu},s}$ can be calculated using the following expression

$$P_{\text{Cu},s} = \frac{Q_s}{2}\hat{i}_s^2 R_{s,\text{coil}} \tag{4}$$

where $R_{s,\mathrm{coil}}$ is the resistance of each stator-slot coil.

The losses of the aluminum squirrel-cage rotor $P_{\mathrm{Al},r}$ can be estimated as follows

$$P_{\mathrm{Al},r} = \frac{Q_r}{2}\hat{\imath}_r^2 R_r \tag{5}$$

subject to

$$R_r = R_b + \frac{2R_{\mathrm{scr}}}{\sin^2\left(\frac{\pi p}{Q_r}\right)} \tag{6}$$

where $\hat{\imath}_r$ is the rotor-bar current amplitude, R_r the equivalent rotor-bar resistance, corresponding to the resistance of one bar and two short-circuit ring elements, R_b the rotor-bar resistance and R_{scr} the resistance of one short-circuit ring element [19].

2. Iron losses: The magnetic flux density in each mesh element κ in the stator and rotor core can be numerically evaluated and approximated as a Fourier series expansion

$$B_\kappa(t) = \sum_{\nu=1}^{\infty} |B_{\kappa,\nu}| \cos\left[\omega_\nu t + \arg\left(B_{\kappa,\nu}\right)\right] \tag{7}$$

where $B_{\kappa,\nu}$ is the complex Fourier coefficient of the magnetic flux density in the mesh element κ and for frequency ν [20]. The stator and rotor iron losses P_{Fe} of the machine can be estimated then as

$$P_{\mathrm{Fe}} L_a \sum_{\kappa=1}^{\kappa_{\max}} \sum_{\nu=1}^{\nu_{\max}} \left\{ k_{\mathrm{e}}\left(|B_{\kappa,\nu}|\right) f_\nu^2 |B_{\kappa,\nu}|^2 + k_{\mathrm{h}}\left(|B_{\kappa,\nu}|\right) f_\nu |B_{\kappa,\nu}|^2 \right\} \Delta_\kappa \tag{8}$$

where Δ_κ is the area of the mesh element κ and k_{e} and k_{h} the eddy-current and hysteresis loss coefficients respectively. These coefficients are assumed to be a function of the magnetic flux density and are expressed as third-order polynomials [21].

3. Mechanical losses: The windage loss component P_w is approximated using the following empirical formula

$$P_w = C_D \pi \rho r_r L_\alpha {\nu_r}^3 \tag{9}$$

subject to

$$\begin{aligned} \sqrt{C_D} &= 2.04 + 1.768 \ln\left(\mathrm{Re}\sqrt{C_D}\right) \\ \mathrm{Re} &= \frac{\rho}{\mu}\omega_m r_r \delta \end{aligned} \tag{10}$$

where C_D is the skin friction coefficient, ρ the air density, ν_r the rotor surface speed, μ the kinematic viscosity of air, Re the Reynolds number and ω_m the angular mechanical frequency [22]. Friction losses are considered negligible.

The efficiency η of each examined pole-phase selection can be determined numerically at each operating point as follows:

$$\eta = \frac{P_m}{P_m + P_{\mathrm{Cu},s} + P_{\mathrm{Al},r} + P_{\mathrm{Fe},s} + P_{\mathrm{Fe},r} + P_w}. \tag{11}$$

where P_m is the mechanical power.

Results and Discussion

In this section, the PPC performance of the designed original 4-pole IM is investigated. For this study, the DC bus voltage limit is set to 550 V. Moreover, the machine is excited up to 2 times the original rated current, as the aim is to focus on the possible benefits of PPC operation at higher-load operation. This high torque capability is feasible for short-time operation, as the saturation on the stator and rotor iron remain on a low level.

Maximum Torque Per Ampere Operation

With maximum torque per ampere operating mode, the torque as well as the torque per ampere capability of all pole-phase selections at $n = 500$ rpm are shown in Fig. 3. For the examined geometry, the torque per ampere capacity of the 2-pole/18-phase configuration starts to saturate already at $\hat{\imath}_s = 5.4$ A, rendering the 4-pole/9-phase operation superior. However, saturation seems to impact the torque output of the 4-pole/9-phase only at the highest examined excitation levels. As a result, the configurations with pole number of 6 or higher do not manage to offer better torque outputs within the examined range, although the 6-pole is very close to overcome the 4-pole selection.

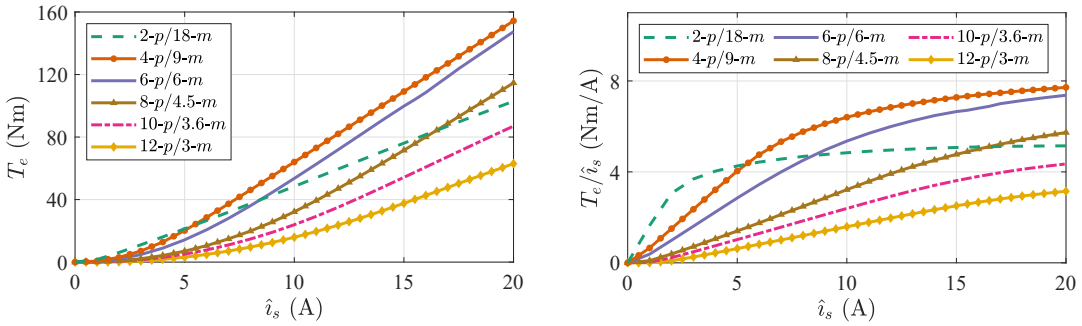

Fig. 3: Plots of $\hat{\imath}_s$ vs (a) torque T_e and (h) $T_e/\hat{\imath}_s$ at $n = 500$ rpm for different pole-phase selections of an original 4-pole machine at maximum torque per ampere operation.

The optimal torque-speed map for maximum torque per ampere operation is shown in Fig. 4. The lowest pole-number operation (i.e. 2-pole/18-phase) significantly widens the flux weakening range compared to a fixed 4-pole operation above 3600 rpm. Specifically, it can be observed in Fig. 5 that pole-phase changing helps to extend the torque-speed envelope significantly at higher speeds, offering an increase equal to 142% in the produced torque per ampere capability at the maximum speed.

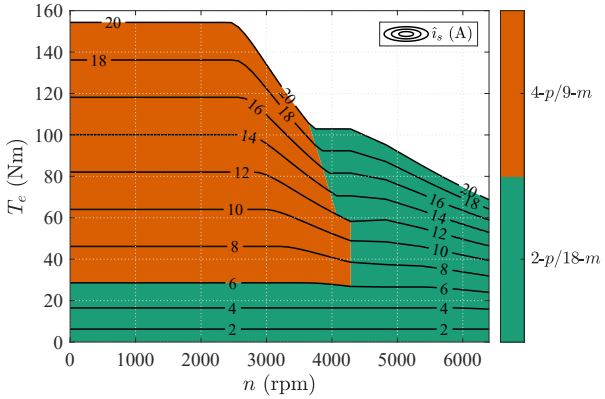

Fig. 4: Optimal torque-speed map of an original 4-pole IM operated as PPC machine at maximum torque per ampere operation for chosen peak current level of $\hat{\imath}_s = 20$ A.

Maximum Efficiency Operation

In this section, the WICSC IM is operated using a maximum efficiency strategy. The total losses P_l, the efficiency η as well as the percentages of stator and rotor losses for the different pole-phase operations

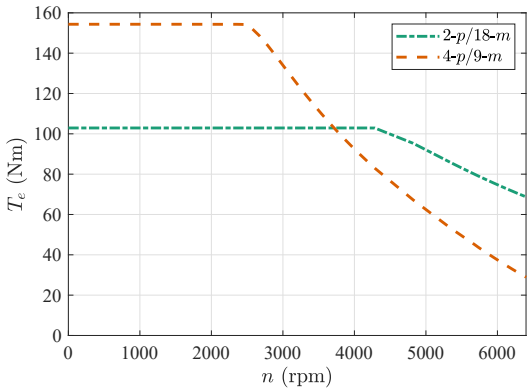

Fig. 5: Torque-speed envelopes of 4-pole/9-phase and 2-pole/18-phase operations of the studied IM with maximum torque per ampere strategy for chosen peak current level of $\hat{\imath}_s = 20$ A.

at $n = 1500$ rpm are shown in Fig. 6 and Fig. 7 respectively. At the examined speed, the total losses of the 4-pole/9-phase operation are the lowest for torque levels higher than $T_e = 45$ Nm, and therefore this pole-phase selection is the most beneficial at the higher range of current excitation levels. Seeing the comparison of stator vs rotor losses shown in Fig. 7, it can be observed that when changing from 2 to 4 poles, the losses shift from the rotor to the stator side. A similar observation is true for the 6-pole/6-phase operation, as it demonstrates higher stator losses and lower rotor losses compared to the 4-pole/9-phase case.

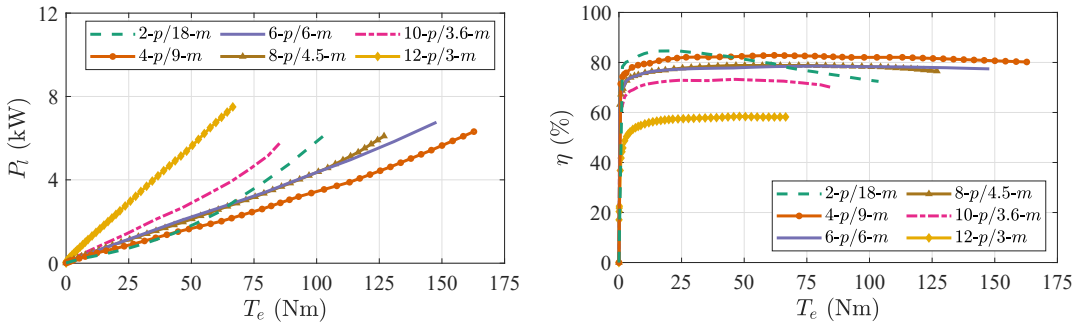

Fig. 6: Plots of T_e vs total losses P_l and η at $n = 1500$ rpm for different pole-phase selections of an original 4-pole machine at maximum efficiency operation.

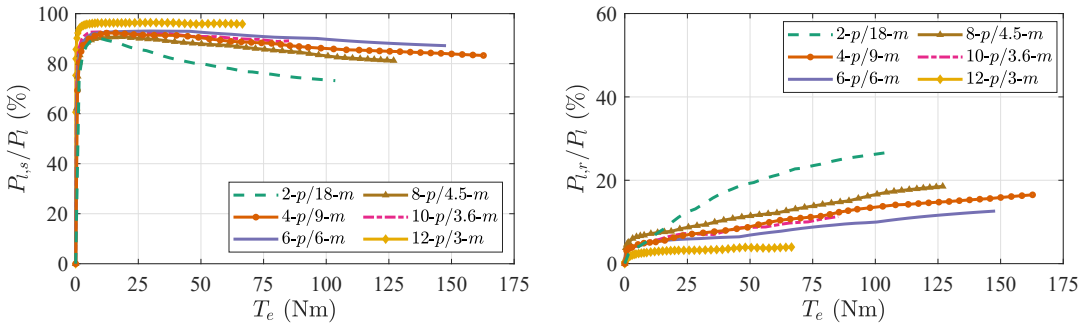

Fig. 7: Plots of T_e vs percentages of stator and rotor losses over total losses, $P_{l,s}/P_l$ and $P_{l,r}/P_l$ respectively, at $n = 1500$ rpm for different pole-phase selections of an original 4-pole IM at maximum efficiency operation.

In Fig. 8, the optimal efficiency map for the whole speed range is depicted.The 2-pole/18-phase operation accomplishes wider flux-weakening range to a noteworthy extent, as wells as improved efficiency at a big part of the lower torque levels. The 4-pole/9-phase operation offers the best efficiency for the highest

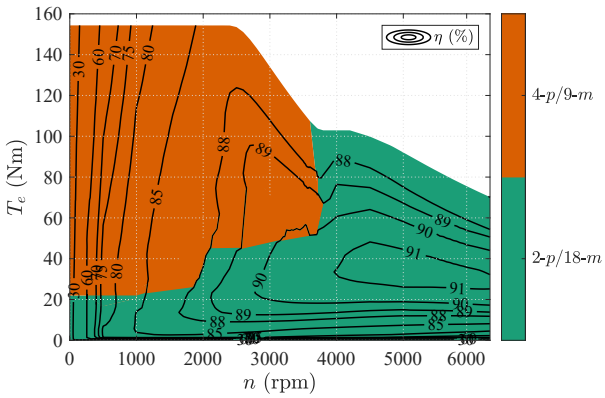

Fig. 8: Optimal efficiency map of an original 4-pole IM operated as PPC machine at maximum efficiency operation for chosen peak current level of $\hat{\imath}_s = 20$ A..

torque capabilities at lower speeds.

Conclusion

The goal of this paper is to examine the impact of pole-phase changing in the performance of an IM topology, originally designed for fixed 4-pole operation. The assessment is carried out focusing on the efficiency and the maximum torque output over the entire speed range. It is shown that by switching to the lowest pole number configuration (i.e. 2-pole/18-phase), a considerable extension of the available torque capability is achieved at higher speeds compared to the 4-pole/9-phase operation, while operation with lower stator current is possible at the lowest load levels. In terms of efficiency, the 2-pole operation is superior at high speed as well as low load conditions, while the 4-pole/9-phase offers the best efficiency for higher torque capabilities at low speeds. The pole-phase combinations with higher pole number than 4 demonstrate poorer performance for the examined excitation range. Further analysis is required in order to assess the influence of the various design variables towards the full utilization of the pole-phase changing capability of IMs.

References

[1] M. V. Terzic, D. S. Mihic and S. N. Vukosavić: Design of High-Speed, Low-Inertia Induction Machines With Drag-Cup Rotor, IEEE Transactions on Energy Conversion, vol. 29, no. 1, pp. 169-177, March 2014.

[2] M. Zeraouila, M. E. H. Benbouzid and D. Diallo: Electric motor drive selection issues for HEV propulsion systems: a comparative study, 2005 IEEE Vehicle Power and Propulsion Conference, 2005.

[3] K. Bitsi, O. Wallmark and S. Bosga, "Many-objective Optimization of IPM and Induction Motors for Automotive Application," 2019 21st European Conference on Power Electronics and Applications (EPE '19 ECCE Europe), 2019, pp. P.1-P.10.

[4] Z. M. Zhao, S. Meng, C. C. Chan and E. W. C. Lo: A novel induction machine design suitable for inverter-driven variable speed systems, IEEE Transactions on Energy Conversion, vol. 15, no. 4, pp. 413-420, Dec. 2000.

[5] J. L. Oldenkamp and S. C. Peak: Selection and Design of an Inverter-Driven Induction Motor for a Traction Drive System, IEEE Transactions on Industry Applications, vol. IA-21, no. 1, pp. 259-265, Jan. 1985.

[6] U. R. Muduli, A. R. Beig, R. K. Behera, K. A. Jaafari and J. Y. Alsawalhi: Predictive Control With Battery Power Sharing Scheme for Dual Open-End-Winding Induction Motor Based Four-Wheel Drive Electric Vehicle, IEEE Transactions on Industrial Electronics, vol. 69, no. 6, pp. 5557-5568, June 2022.

[7] M. Oh and I. Husain: Optimal Torque Distribution of Dual-Motor All-Wheel Drive Electric Vehicles for Maximizing Motor Energy Efficiency, 2021 IEEE Transportation Electrification Conference & Expo (ITEC), 2021, pp. 188-193.

[8] M. Osama and T. A. Lipo: A new inverter control scheme for induction motor drives requiring wide speed range, IAS '95. Conference Record of the 1995 IEEE Industry Applications Conference Thirtieth IAS Annual Meeting, 1995.

[9] S. Mallampalli, Z. Q. Zhu, J. C. Mipo and S. Personnaz: Six-Phase Pole-Changing Winding Induction Machines With Improved Performance, IEEE Transactions on Energy Conversion, vol. 36, no. 1, pp. 534-546, March 2021.

[10] M. P. Magill and P. T. Krein: A dynamic pole-phase modulation induction machine model, 2015 IEEE International Electric Machines & Drives Conference (IEMDC), 2015, pp. 13-19.
[11] H. Yano and K. Sakai: Integrated Motor-Controlled Independently by Multi-Inverters with Pole and Phase Changes, 2019 21st European Conference on Power Electronics and Applications (EPE '19 ECCE Europe), 2019, pp. P.1-P.10.
[12] K. Bitsi, O. Wallmark and S. Bosga: An Induction Machine with Wound Independently-Controlled Stator Coils, 2019 22nd International Conference on Electrical Machines and Systems (ICEMS), 2019, pp. 1-5.
[13] O. Wallmark, K. Bitsi and S. G. Bosga, "A Transient Model of WICSC and ISCAD Machines Based on Permeance Networks," 2020 International Conference on Electrical Machines (ICEM), 2020, pp. 2048-2054.
[14] A. Boglietti, A. Cavagnino, M. Lazzari, and S. Vaschetto: Preliminary induction motor electromagnetic sizing based on a geometrical approach, IET Electric Power Applications, vol. 6, no. 9, pp. 583–592, November 2012.
[15] P. Ponomarev, Y. Alexandrova, I. Petrov, P. Lindh, E. Lomonova, and J. Pyrhönen: Inductance calculation of tooth-coil permanent-magnet synchronous machines, IEEE Transactions on Industrial Electronics, vol. 61, no. 11, pp. 5966–5973, 2014.
[16] S. Williamson and M. A. Muller: Calculation of the impedance of rotor cage end rings, IEE proceedings.-B, vol. 140, no. 1, p. 51, 1993.
[17] T. Murata, T. Tsuchiya and I. Takeda: Vector control for induction machine on the application of optimal control theory, IEEE Transactions on Industrial Electronics, vol. 37, no. 4, pp. 283-290, Aug. 1990.
[18] H. Cai, L. Gao and L. Xu: Calculation of Maximum Torque Operating Conditions for Inverter-Fed Induction Machine Using Finite-Element Analysis, IEEE Transactions on Industrial Electronics, vol. 66, no. 4, pp. 2649-2658, April 2019.
[19] T. Lipo: Introduction to AC Machine Design, ser. IEEE Press Series on Power Engineering. Wiley, 2017.
[20] O. Wallmark and K. Bitsi: Iron-loss computation using matlab and comsol multiphysics, 2020 International Conference on Electrical Machines (ICEM), vol. 1, 2020, pp. 916–920.
[21] A. Boglietti, A. Cavagnino, D. M. Ionel, M. Popescu, D. A. Staton, and S. Vaschetto: A general model to predict the iron losses in pwm inverterfed induction motors, IEEE Transactions on Industry Applications, vol. 46, no. 5, pp. 1882–1890, 2010.
[22] C. T. Krasopoulos, M. E. Beniakar, and A. G. Kladas: Multicriteria pm motor design based on anfis evaluation of ev driving cycle efficiency, IEEE Transactions on Transportation Electrification, vol. 4, no. 2, pp. 525–535, 2018.